Journal of the Optical Society of America B
OPTICAL PHYSICS

Bandwidth tunable microstrip band-stop filters based on localized spoof surface plasmons

Bingzheng Xu,[1] Zhuo Li,[1,2,3,*] Liangliang Liu,[1] Jia Xu,[1] Chen Chen,[1] and Changqing Gu[1]

[1]Key Laboratory of Radar Imaging and Microwave Photonics, Ministry of Education, College of Electronic and Information Engineering, Nanjing University of Aeronautics and Astronautics, Nanjing 211106, China
[2]State Key Laboratory of Millimeter Waves, Southeast University, Nanjing 210096, China
[3]Department of Physics, College of Liberal Arts and Sciences, Arizona State University, Arizona 871504, USA
*Corresponding author: lizhuo@nuaa.edu.cn

Received 30 March 2016; revised 16 May 2016; accepted 18 May 2016; posted 19 May 2016 (Doc. ID 262069); published 7 June 2016

In this work, a bandwidth tunable microstrip band-stop filter is theoretically investigated and experimentally verified based on the concept of localized spoof surface plasmons. By placing a conventional microstrip at the bottom center of a symmetrically periodically corrugated metallic strip, which supports spoof surface plasmons with a single defect or a series of defects of continuously variable dimensions, localization of the quasi-static field propagating along the microstrip can be realized, thus facilitating control of the central frequency, bandwidth, and absorption level of the microstrip band-stop filter. A band-notched microstrip and a band-stop one are cautiously designed and verified through simulations and experiments, which can find potential applications in microwave band-stop circuits.

OCIS codes: (050.6624) Subwavelength structures; (240.6680) Surface plasmons; (350.4010) Microwaves; (070.2615) Frequency filtering.

http://dx.doi.org/10.1364/JOSAB.33.001388

1. INTRODUCTION

Surface plasmons (SPs) are electromagnetic waves that exist at the interface between the metal-dielectric of opposite signs in electric permittivities at infrared or visible frequency [1]. The SPs present high spatial confinement by significantly reducing the effective wavelength of surface waves [2]. In general, SPs originally exist in two types of modes: one is the propagation mode at the interface of metal and dielectric, named surface plasmon polaritons (SPPs) [3]; the other is the resonance mode on subwavelength metal particles, named localized surface plasmons (LSPs) [4]. When the frequency is reduced to THz and microwave bands, it is difficult to excite SPPs and LSPs because noble metals turn out to be good conductors instead of dielectrics with negative permittivity [5]. To realize high-confinement at lower frequencies, an effective approach is to pattern a metal surface with periodical grooves or holes, which may significantly improve the confinement of SPPs and LSPs even in the PEC limit [6–10].

Ultrathin corrugated metallic strips have been proposed to support conformal surface plasmons (CSPs) on curved surfaces or spoof SPPs on planar paths, leading to various ultrathin microwave and THz plasmonic functional devices [11–15]. Spoof LSPs were found to be supported on a 2D periodically textured metallic cylinder [16–18]. Magnetic LSPs supported by cylindrical structures were then theoretically and experimentally explored in [19]. Later on, high-order spoof LSPs in periodically corrugated metal particles also were investigated in [20]. Liao *et al.* [21] proposed a compact combined system to support compound resonances with the coupling between spoof LSPs and SPPs, which may find potential applications in sensing and integrated photonic circuitry. Recently, by introducing a defect on grooved metallic arrays, a localized subwavelength surface defect mode that emerges in the bandgap was realized in the microwave regime [22]. Borrowing the same idea, narrow or multiple narrow stop bands have been generated flexibly and conveniently in a conventional coplanar waveguide by introducing one or more defect units into the ultrathin periodic corrugated metallic strips on the back of the substrate [23].

In this work, we design a bandwidth tunable microstrip band-stop filter by adding a subwavelength periodic corrugated metal strip with defect units on top of a conventional microstrip. The defect mode exists in the bandgap between the fundamental and the first higher mode of the spoof surface plasmons that are supported on this corrugated metal strip, which can be introduced to form a stop band. When a series of defects with continuously variable dimensions are introduced in the spoof SPPs waveguide, they will arouse strong and continuous coupling with the microstrip, resulting in a broad stop band in the microstrip bandwidth. It is interesting to note that the absorption level and center frequency of each stop band could be

adjusted conveniently, thus making it possible to get a broad stop-band filter with a series of continuously variable dimensioned defects. Both theoretical analysis and experimental results validate our idea, which have important applications in band-stop circuits and systems. This structure is of simple configuration, low profile, and frequency tunability and can find wide applications in the band-notched devices in the plasmonic and microwave circuit.

2. ANAYLSIS AND DISCUSSION

To begin with, we shall first briefly look at this band-stop microstrip filter, which is a two-layered structure fabricated separately at a lower price. The upper layer consists of corrugated metallic strips and substrate, which can support spoof SPPs modes, and the lower layer is a conventional microstrip line. Figures 1(a) and 1(b) show the top view of two kinds of corrugated metal strips, which have two types of shapes, namely I and II, and Fig. 1(c) illustrates the top view of the microstrip line. For the upper layer, the ultrathin metallic strips are copper, and the supporting substrate (Rogers 6010) is 0.635 mm thick. For the lower layer, the width of the microstrip signal line $w_2 = 3.1$ mm, and the supporting substrates (Rogers 5880) is 1 mm thick. Both copper layers are of 0.018 mm height and with a conductivity of 5.8×10^7 S/m. Figure 1(d) presents the cross section of the two-layered structure.

We first study the unit cell of the compound structure, in which the period, width, and depth of grooves are designed as $p = 3$ mm, $d = 2.5$ mm, and $h_1 = 2.6$ mm, respectively. To investigate the propagation features of the SPPs mode, we first study the dispersion relation of two composite structures, as shown in Fig. 2 for two different groove shapes (marked I and II). Compared with Shape I, Shape II adds a orthogonal strip at the end of the strip forming a T-shaped strip, with the dimension $a = 2$ mm and $b = 0.2$ mm. It is obvious that the SPPs are in the nonradiative region, capable of confining EM waves

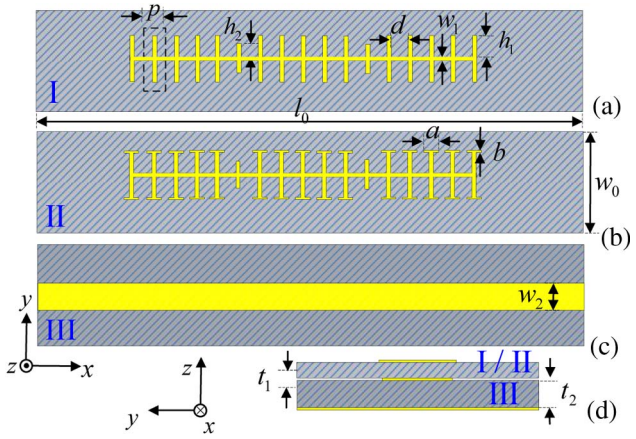

Fig. 1. Schematic configuration of the band-stop microstrip filter. (a) Top view of the corrugated metallic strip, in which the length and width of this layer are $l_0 = 60$ mm and $w_0 = 15$ mm. The unit cell of the strip is designed as $p = 3$ mm $d = 2.5$ mm, $w_1 = 0.2$ mm $h_1 = 2.6$ mm. (b) Top view of the corrugated strip of T shape. (c) Top view of the microstrip signal line with the width $w_2 = 3.1$ mm. (d) Side-view cross section of the whole model. The corrugated metallic strip (I or II) is right above the microstrip line (III).

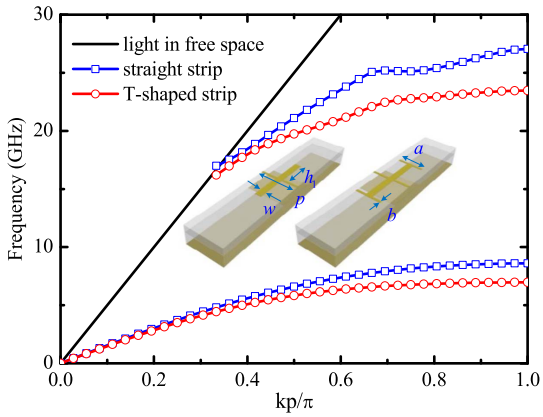

Fig. 2. Dispersion curves of the fundamental and first higher mode spoof SPPs modes for two kinds of corrugated metallic strips, in which the blue line corresponds to the straight strip and the red line corresponds to the T-shaped strip. The inset shows the corresponding two shape unit cell.

on the surface. And there is a bandgap between the fundamental and the first higher mode of the spoof SPPs with both bands deviating significantly from the light line. The asymptotic frequencies of the fundamental and the first higher mode for the T-shaped strip is lower than the straight strip owing to the extension part, which actually increases the effective height of the groove.

With this photonic crystal bandgap in [22], the localized spoof SPPs can be excited by introducing a point defect in the spoof SPPs waveguide. The defect unit can be chosen arbitrarily with any unit cell displaced with a shorter one ($h_2 < h_1$). To demonstrate the transmission performance quantitatively, Fig. 3 gives the simulated S parameters of Shapes I and II. It can be seen that the band-notched function of the straight strip (Shape I) is much weaker than the T-shaped strip (Shape II). Thus, in the following design, we only focus on the T-shaped strip. The whole width of the strip is $2h_1 + w_1$ and slightly larger than the signal linewidth $w_2 = 3.1$ mm, which is designed to match a 50 Ω input impedance. Two same defects form a very narrow dip at about 7 GHz in the whole transmission spectrum of the microstrip, shown as the solid red line in Fig. 3(b), demonstrating an excellent band-notched property in a narrow frequency regime. As mentioned in [23], the strong coupling between the spoof SPPs waveguide and the microstrip also will affect the transmission efficiency outside the bandgap, in which several small dips occur, which can be minimized by tuning the dimensions of the corrugated strips and the dielectric thickness of the upper layer. The simulated field distributions of the E_z component on the surface of the microstrip at the dip (about 7 GHz) are depicted in Fig. 3(d), exhibiting strong field confinement and localization around the defects. In addition, for the signal fed at the input port (left-hand side), the electromagnetic energy was absorbed one by one passing through the two defects along the transmission direction, indicating that, if much stronger absorption is wanted, more defects should be included with the same dimension.

To further evaluate the operation performance quantitatively, we fabricated the structure, as shown in the inset of

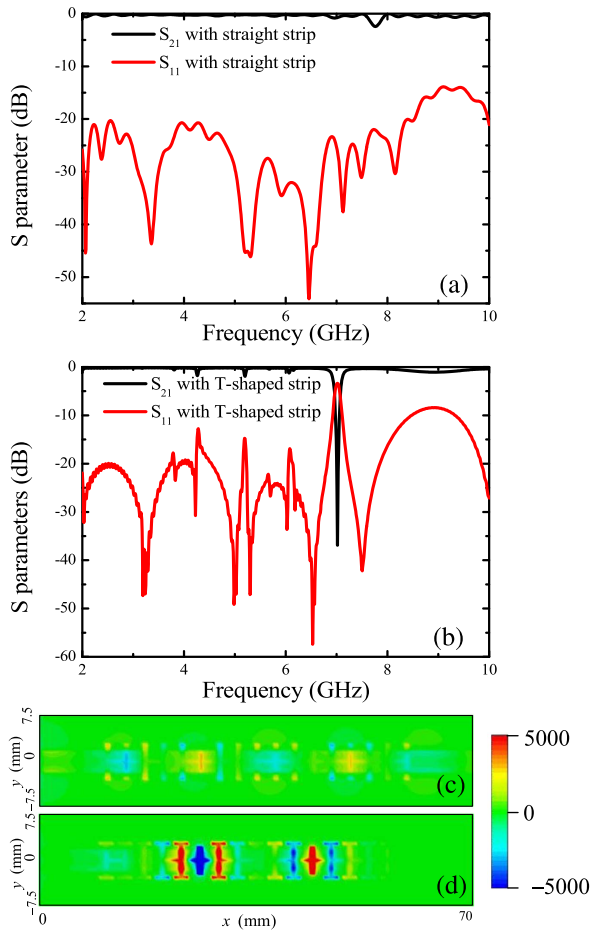

Fig. 3. (a), (b) Simulated S parameters of the structure for two different shape strips with two similar defects ($h_2 = 2.0$ mm). (c), (d) Simulated electric field distributions at two defects of different shape strips I and II at the rejection frequency.

Fig. 4. Two coaxial cables with 50 Ω port impedances are connected to both ends of the microstrip sample via SMA connectors. And two defects of the same groove height $h_2 = 2.0$ mm are designed with five periods in between. Figure 4 shows the simulation results of the S parameters in solid lines as well as the experimental ones (in dashed lines). We note that the proposed microstrip structure provides an excellent band-notched function at 7 GHz within the propagating band. The center frequency of the stop bands is in excellent agreement with the full-wave simulations. Although there exists a discrepancy between the simulated and measured curves due to the misaligned position of the two-layered structure during the experiment, the proof-of-concept experiment validates our idea. And the proposed corrugated strip with defects has excellent band-filtering characteristics.

Inspired by the design above, in this section, we further demonstrate that a broad stop-band microstrip filter could be realized by placing a series of defects with continuously variable dimensions on the upper layer, which can be explained that these defects actually introduce a band-notch function at a series of discrete frequencies forming a relatively broad stop-band bandwidth. First, to quantitatively evaluate the

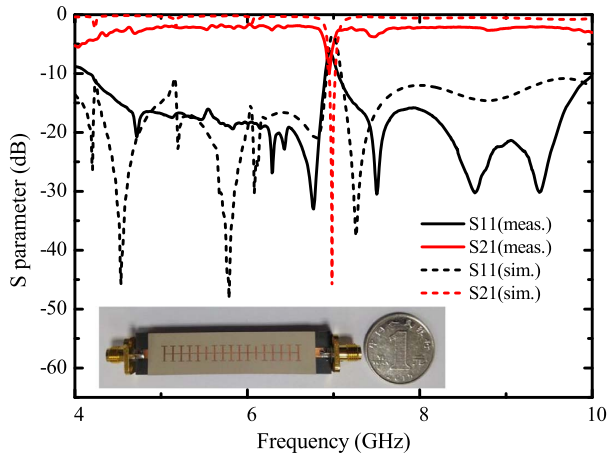

Fig. 4. Simulated (dotted lines) and measured (solid lines) S parameters of the structure with two similar defects ($h_2 = 2.0$ mm). The fabricated structure is shown in the inset.

performance of the band-stop microstrip filter, we calculated the S parameter of the structure in Fig. 5(a) with seven defects of specific dimensions. As shown in Fig. 5(a), seven

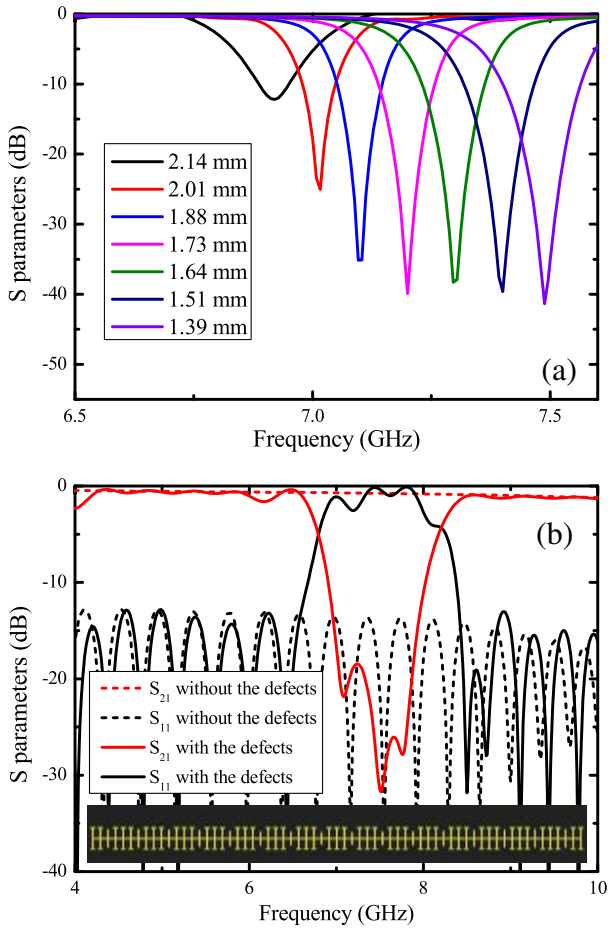

Fig. 5. (a) Transmission spectrum (S_{21}) of the structure for various defect heights h_2. (b) Simulated transmission coefficient S_{21} and reflection coefficients S_{11} for the broadband case. Bottom inset: the schematic picture of the broadband band-stop filter.

different defect heights ($h_2 = 2.14$, 2.01, 1.88, 1.73, 1.64, 1.51, and 1.39 mm) with nonuniform variations are cautiously optimized to form seven narrow dips at seven equally spaced frequencies at 6.9, 7.0, 7.1, 7.2, 7.3, 7.4, and 7.5 GHz, facilitating the realization of high-performance band-stop characteristics in the specified frequency range. We remark that different criteria for choosing the defect height can be used to control wide-band rejection beside this one. In Fig. 5(a), the solid lines in different colors correspond to the transmission coefficients S_{21} of the band-notched microstrips with different defect heights h_2, which are designed to form an approximately stop band from 6.9 to 7.5 GHz. Additionally, we also can observe that the band-notched frequency is controlled and can be adjusted by the height h_2. When h_2 approaches h_1, the absorption energy of the localized spoof SPPs becomes the weakest, thus leading to a shallow dip on the S_{21} curve. From Fig. 5(a), we also can observe that one single defect could only lead to a narrow notched band. Thus, to realize a high absorption level in a wide frequency band, the whole bandwidth should be first divided into N equally spaced frequency intervals of about 100 MHz. Then, the height of each defect unit should be optimized to get a dip at the center frequency of each interval. In order to get a high rejection level at each frequency, two defect units of the same dimensions are used, leading to $2N$ ($N = 7$) defect units as a whole. However, as shown in Fig. 5(a), the absorption level is relatively weak when $h_2 = 2.14$ mm, two more defects with $h_2 = 2.14$ mm are added to form a totally 16 defect unit broadband band-stop microstrip filter in the inset of Fig. 5(b). The simulation results of the transmission coefficients (S_{21}) and reflection coefficients (S_{11}) illustrated in Fig. 5(b) demonstrate that a rejection bandwidth of 1.1 GHz with $S_{21} < -10$ dB.

3. CONCLUSIONS

In summary, we have theoretically proposed a compact microstrip band-stop filter and verified it experimentally based on localized spoof surface plasmons. By tuning the dimensions and the number of the defect units, single or wide stop bands could be conveniently introduced. The subwavelength metallic strips, which can support spoof plasmons, play an important role in the structure. Numerical simulations and experimental results are provided to verify the above phenomena. In addition, this type of band-notched structure based on localized spoof surface plasmons is easy to design and fabricate. In this framework, we can realize tunable frequency-rejection devices in the microwave and terahertz frequencies.

Funding. Natural Science Foundation of Jiangsu Province (BK20151480); Foundation of State Key Laboratory of Millimeter Waves, Southeast University, China (K201603); Funding of Jiangsu Innovation Program for Graduate Education (KYLX 0276); Funding for Outstanding Doctoral Dissertation in NUAA (BCXJ15-04); Fundamental Research Funds for the Central Universities (NS2016039); China Scholarship Council (CSC).

REFERENCES

1. W. L. Barnes, A. Dereux, and T. W. Ebbesen, "Surface plasmon subwavelength optics," Nature **424**, 824–830 (2003).
2. J. M. Pitarke, V. M. Silkin, E. V. Chulkov, and P. M. Echenique, "Theory of surface plasmons and surface-plasmon polaritons," Rep. Prog. Phys. **70**, 1–87 (2007).
3. T. W. Ebbesen, C. Genet, and S. I. Bozhevolnyi, "Surface-plasmon circuitry," Phys. Today **61**, 44–50 (2008).
4. K. A. Willets and R. P. Van Duyne, "Localized surface plasmon resonance spectroscopy and sensing," Annu. Rev. Phys. Chem. **58**, 267–297 (2007).
5. G. Kumar, A. Cui, S. Pandey, and A. Nahata, "Planar terahertz waveguides based on complementary split ring resonators," Opt. Express **19**, 1072–1080 (2011).
6. J. B. Pendry, L. Martin-Moreno, and F. J. Garcia-Vidal, "Mimicking surface plasmons with structured surfaces," Science **305**, 847–848 (2004).
7. A. P. Hibbins, B. R. Evans, and J. R. Sambles, "Experimental verification of designer surface plasmons," Science **308**, 670–672 (2005).
8. Q. Gan, Z. Fu, Y. J. Ding, and F. J. Bartoli, "Ultrawide-bandwidth slow-light system based on THz plasmonic graded metallic grating structures," Phys. Rev. Lett. **100**, 256803 (2008).
9. D. Martin-Cano, M. L. Nesterov, A. I. Fernandez-Dominguez, F. J. Garcia-Vidal, L. Martin-Moreno, and E. Moreno, "Plasmons for subwavelength terahertz circuitry," Opt. Express **18**, 754–764 (2010).
10. X. Gao, J. H. Shi, X. P. Shen, H. F. Ma, W. X. Jiang, L. M. Li, and T. J. Cui, "Ultrathin dual-band surface plasmonic polariton waveguide and frequency splitter in microwave frequencies," Appl. Phys. Lett. **102**, 151912 (2013).
11. X. P. Shen, T. J. Cui, D. Martin-Cano, and F. J. Garcia-Vidal, "Conformal surface plasmons propagating on ultrathin and flexible films," Proc. Natl. Acad. Sci. **110**, 40–45 (2013).
12. X. P. Shen and T. J. Cui, "Planar plasmonic metamaterial on a thin film with nearly zero thickness," Appl. Phys. Lett. **102**, 211909 (2013).
13. R. Quesada, D. Martin-Cano, F. J. Garcia-Vidal, and J. Bravo-Abad, "Deep-subwavelength negative-index waveguiding enabled by coupled conformal surface plasmons," Opt. Lett. **39**, 2990–2993 (2014).
14. I. R. Hooper, B. Tremain, J. A. Dockrey, and A. P. Hibbins, "Massively sub-wavelength guiding of electromagnetic waves," Sci. Rep. **4**, 7495 (2014).
15. A. Kianinejad, Z. N. Chen, and C. W. Qiu, "Design and modeling of spoof surface plasmon modes-based microwave slow-wave transmission line," IEEE Trans. Microw. Theory Tech. **63**, 1817–1825 (2015).
16. A. Pors, E. Moreno, L. Martin-Moreno, J. B. Pendry, and F. J. Garcia-Vidal, "Localized spoof plasmons arise while texturing closed surfaces," Phys. Rev. Lett. **108**, 223905 (2012).
17. Z. Li, B. Z. Xu, C. Q. Gu, P. P. Ning, L. L. Liu, Z. Y. Niu, and Y. J. Zhao, "Localized spoof plasmons in closed textured cavities," Appl. Phys. Lett. **104**, 251601 (2014).
18. B. Z. Xu, Z. Li, C. Q. Gu, P. P. Ning, L. L. Liu, Z. Y. Niu, and Y. J. Zhao, "Multi-band localized spoof plasmons in closed textured cavities," Appl. Opt. **53**, 6950–6953 (2015).
19. X. P. Shen and T. J. Cui, "Magnetic localized surface plasmons," Laser Photon. Rev. **8**, 137–145 (2014).
20. B. Y. Yang, Y. J. Zhou, and Q. X. Xiao, "Spoof localized surface plasmons in corrugated ring structures excited by microstrip line," Opt. Express **23**, 21434–21442 (2015).
21. Z. Liao, X. Shen, B. C. Pan, J. Zhao, Y. Luo, and T. J. Cui, "Combined system for efficient excitation and capture of LSP resonances and flexible control of SPP transmissions," ACS Photon. **2**, 738–743 (2015).
22. S. Kim, S. Oh, K. Kim, J. Kim, H. Park, W. Hess, and C. Kee, "Subwavelength localization and toroidal dipole moment of spoof surface plasmon polaritons," Phys. Rev. B **91**, 035116 (2015).
23. B. Z. Xu, Z. Li, L. L. Liu, J. Xu, C. Chen, P. Ning, X. Chen, and C. Q. Gu, "Tunable band-notched coplanar waveguide based on localized spoof surface plasmons," Opt. Lett. **40**, 4683–4686 (2015).